Periostin limits tumor response to VEGFA inhibition.

Ionna Keklikoglou, Ece Kadioglu, Stefan Bissinger, B Langlois, Axel Bellotti, Gertraud Orend, Carola H Ries, Michele de Palma

Report

Cell Reports

Periostin Limits Tumor Response to VEGFA Inhibition

Graphical Abstract

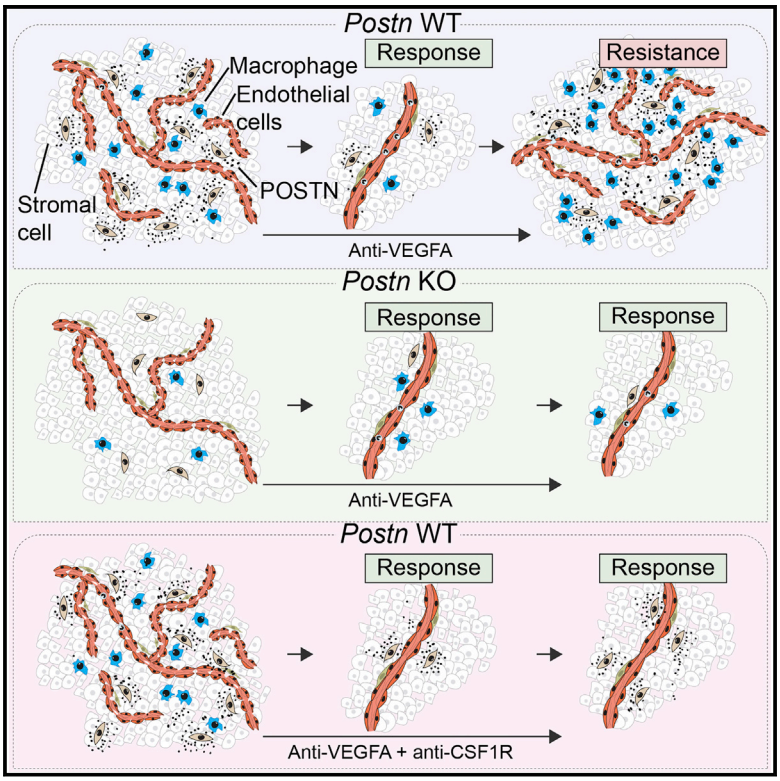

Highlights

- VEGFA inhibition acutely abates stromal cells and POSTN in PNETs
- Revascularization is associated with POSTN deposition and macrophage infiltration
- Genetic *Postn* inactivation extends PNET response to VEGFA blockade
- PNET response to VEGFA inhibition can be enhanced through macrophage elimination

Authors

Ioanna Keklikoglou, Ece Kadioglu, Stefan Bissinger, ..., Gertraud Orend, Carola H. Ries, Michele De Palma

Correspondence

michele.depalma@epfl.ch

In Brief

The molecular and cellular mechanisms underlying tumor resistance to VEGFA neutralization are diverse and incompletely understood. Keklikoglou et al. show that *de novo* deposition of the matrix protein periostin (POSTN) orchestrates tumor adaptation to chronic VEGFA inhibition by sustaining macrophage infiltration in a mouse model of pancreatic neuroendocrine tumor (PNET).

Keklikoglou et al., 2018, Cell Reports *22*, 2530–2540
March 6, 2018
https://doi.org/10.1016/j.celrep.2018.02.035

CellPress

OPEN ACCESS
CellPress

Cell Reports
Report

Periostin Limits Tumor Response to VEGFA Inhibition

Ioanna Keklikoglou,[1] Ece Kadioglu,[1] Stefan Bissinger,[2] Benoît Langlois,[3,4,5] Axel Bellotti,[1] Gertraud Orend,[3,4] Carola H. Ries,[2] and Michele De Palma[1,6,*]

[1]Swiss Institute for Experimental Cancer Research (ISREC), School of Life Sciences, École Polytechnique Fédérale de Lausanne (EPFL), 1015 Lausanne, Switzerland

[2]Roche Innovation Center Munich, Roche Pharma Research and Early Development, 82377 Penzberg, Germany

[3]INSERM U1109, MN3T, The Microenvironmental Niche in Tumorigenesis and Targeted Therapy, 3 Avenue Moliere, 67200 Strasbourg, France

[4]Université de Strasbourg, 67000 Strasbourg, France

[5]Present address: INSERM U1109, ImmunoRheumatologie Moléculaire (IRM), Hopital Civil, Institut d'Hématologie et d'Immunologie, 1 Place de l'Hôpital, 67091 Strasbourg, France

[6]Lead Contact

*Correspondence: michele.depalma@epfl.ch

https://doi.org/10.1016/j.celrep.2018.02.035

SUMMARY

Resistance to antiangiogenic drugs limits their applicability in cancer therapy. Here, we show that revascularization and progression of pancreatic neuroendocrine tumors (PNETs) under extended vascular-endothelial growth factor A (VEGFA) blockade are dependent on periostin (POSTN), a matricellular protein expressed by stromal cells. Genetic deletion of *Postn* in RIP1-Tag2 mice blunted tumor rebounds of M2-like macrophages and αSMA$^+$ stromal cells in response to prolonged VEGFA inhibition and suppressed PNET revascularization and progression on therapy. POSTN deficiency also impeded the upregulation of basic fibroblast growth factor (FGF2), an adaptive mechanism previously implicated in PNET evasion from antiangiogenic therapy. Higher *POSTN* expression correlated with markers of M2-like macrophages in human PNETs, and depleting macrophages with a colony-stimulating factor 1 receptor (CSF1R) antibody inhibited PNET revascularization and progression under VEGFA blockade despite continued POSTN production. These findings suggest a role for POSTN in orchestrating resistance to anti-VEGFA therapy in PNETs.

INTRODUCTION

Vascular endothelial growth factor A (VEGFA) sustains tumor angiogenesis by engaging the VEGF receptor (VEGFR) 2 expressed on vascular endothelial cells (ECs). The clinical benefits of adding bevacizumab, a VEGFA monoclonal antibody (mAb), to first-line anti-cancer therapies are, however, generally modest (Ferrara and Adamis, 2016). This can be attributed to compensatory proangiogenic signaling that may rescue angiogenesis under VEGFA deprivation (Bergers and Hanahan, 2008; Casanovas et al., 2005; Rigamonti et al., 2014), as well as tumor adaptation to decreased angiogenesis, which may involve metabolic reprogramming or enhanced growth along preexisting blood vessels (Allen et al., 2016; Frentzas et al., 2016). Also, myeloid cells like macrophages and neutrophils may limit antiangiogenic therapy by producing alternative proangiogenic and survival factors for ECs in VEGFA-depleted microenvironments (Bergers and Hanahan, 2008; De Palma and Lewis, 2013; De Palma et al., 2017; Rivera and Bergers, 2015; Shojaei and Ferrara, 2008).

The extracellular matrix (ECM) modulates tumor angiogenesis and response to antiangiogenic therapy (De Palma et al., 2017; Egeblad et al., 2010; Rahbari et al., 2016; Stylianopoulos et al., 2012; Van Obberghen-Schilling et al., 2011). Periostin (POSTN), a matricellular protein expressed primarily by mesenchymal-lineage cells, promotes tumor angiogenesis, invasion, and metastasis by stimulating cancer cell and EC proliferation and migration (Bao et al., 2004; Chen et al., 2017; Hu et al., 2016; Kikuchi et al., 2014; Liu et al., 2014; Naba et al., 2017; Park et al., 2016; Shao et al., 2004; Takanami et al., 2008; Underwood et al., 2015; Zhou et al., 2015; Zhu et al., 2010). In a mouse glioma model, POSTN was shown to recruit and activate M2-like macrophages (Zhou et al., 2015), which have proangiogenic capacity (De Palma and Lewis, 2013). The diverse protumoral functions of POSTN may, therefore, antagonize the efficacy of antiangiogenic treatments. In this study, we examined the effects of genetically inactivating *Postn* in pancreatic neuroendocrine tumors (PNETs) of transgenic RIP1-Tag2 mice (Casanovas et al., 2005; Rigamonti et al., 2014) treated with a mouse VEGFA mAb equivalent to bevacizumab.

RESULTS

POSTN Is Associated with the Angiogenic Switch and On-Therapy Re-vascularization in Mouse PNETs

We used the B20-4.1.1 ("B20") mAb (Liang et al., 2006) to block VEGFA signaling in 11-week-old RIP1-Tag2 transgenic mice carrying early established PNETs (Casanovas et al., 2005; Rigamonti et al., 2014). We employed two weekly doses of B20 (10 or 20 mg/kg) and analyzed the pancreata at distinct time points (1.5, 2.5, 4, and 6 weeks) post-therapy initiation (PTI) by

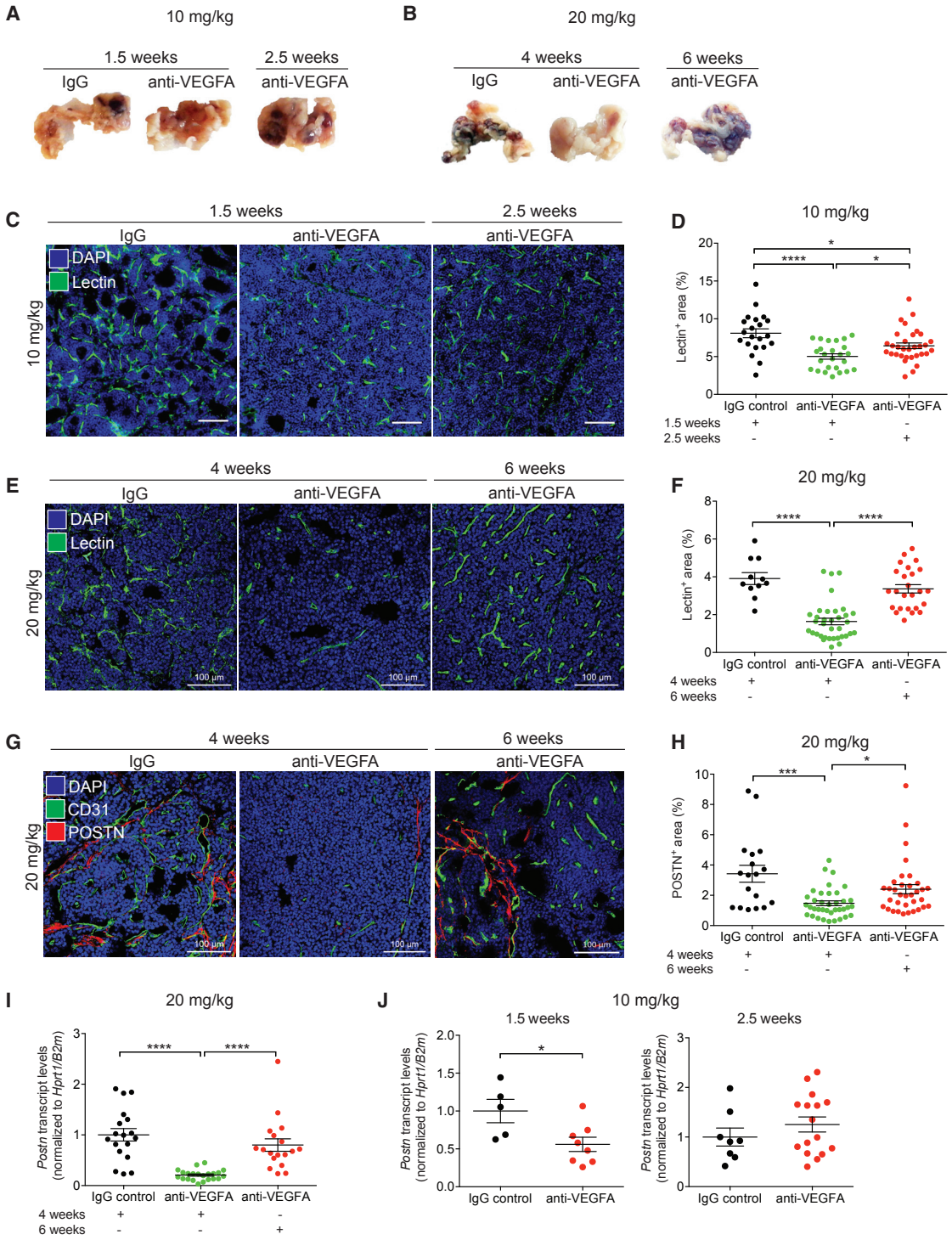

Figure 1. POSTN Expression Is Associated with Rebound Angiogenesis in PNETs

(A and B) Representative photos of pancreata of 12.5- to 17-week-old RIP1-Tag2 mice, treated as indicated. Dark lesions represent hemorrhagic PNETs.

(C and E) Representative images of perfused lectin (green) and DAPI (blue) nuclear staining in PNETs of either 12.5- to 13.5-week-old (C) or 15- to 17-week-old (E) mice. Scale bar, 100 µm.

(D and F) Relative lectin$^+$ vascular area (mean percentage values ± SEM) in PNETs of 12.5- to 13.5-week-old (D) or 15- to 17-week-old (F) mice. (D) IgG control (1.5 weeks PTI): n = 21 tumors from 3 mice; anti-VEGFA (1.5 weeks PTI): 25 from 4 mice; anti-VEGFA (2.5 weeks PTI): n = 32 from 4 mice. (F) IgG control

(legend continued on next page)

both gross morphology (Figures 1A and 1B) and immunostaining of pancreatic sections to identify perfused blood vessels (Figures 1C–1F). The kinetics of PNET response to B20 was dose dependent; whereas tumors in the 10 mg/kg dose group revascularized at 2.5 weeks PTI after a short-lived antiangiogenic response, those in the 20 mg/kg dose group revascularized at 6 weeks PTI after a more extended antiangiogenic response. To maximize the therapeutic window, we employed a B20 dosage regimen of 20 mg/kg per week in subsequent experiments, unless stated otherwise.

POSTN has been associated with tumor angiogenesis (Chen et al., 2017) and is highly expressed in the AngioMatrix dataset of proteins upregulated during the angiogenic switch of PNETs (Langlois et al., 2014). However, it is unknown whether it also sustains PNET revascularization during anti-VEGFA therapy. qPCR analysis of pancreatic islets isolated from RIP1-Tag2 mice between 6 and 13 weeks of age revealed significant upregulation of *Postn* at 8 weeks of age (Figure S1), a time point when dysplastic islets transition to overt tumors through an angiogenic switch (Bergers et al., 2000). We then examined POSTN expression in B20-treated PNETs harvested either at the response (4 weeks PTI) or revascularization (6 weeks PTI) phase by immunostaining (Figures 1G and 1H) and qPCR (Figure 1I). Both analyses showed marked POSTN reduction during the response (antiangiogenic) phase, followed by its increase to quasi-baseline levels during the revascularization phase. We observed a similar kinetics of *Postn* expression in PNETs of mice that had received B20 at 10 mg/kg per week and that were analyzed at 1.5 and 2.5 weeks PTI (Figure 1J). These findings indicate that in B20-treated PNETs, transient vascular attrition and subsequent revascularization are respectively associated with the demise and recovery of POSTN deposition.

POSTN Is Expressed by Stromal Cells and Limits PNET Response to Anti-VEGFA Therapy

Previous studies have shown that in tumors, POSTN is largely expressed by stromal cells encompassing fibroblasts and pericytes (Kikuchi et al., 2014; Underwood et al., 2015). In PNETs, POSTN co-localized with α-smooth muscle actin (αSMA)$^+$ cells (Figures 2A and 2B), which identify both fibroblasts and pericytes in this tumor model (Sugimoto et al., 2006). Accordingly, PDGFRα^+CD45$^-$ stromal cells sorted from PNETs of either immunoglobulin G (IgG)- or B20-treated mice robustly expressed *Postn*, whereas ECs (CD31$^+$CD45$^-$), macrophages (CD45$^+$CD11b$^+$F4/80$^+$), and enriched cancer cells (CD45$^-$CD31$^-$PDGFRα^-) expressed it at negligible levels (Figures 2C and S2A–S2C).

The kinetics of stromal cell abundance paralleled that of POSTN in B20-treated PNETs. Indeed, αSMA$^+$ stromal cells dramatically declined during the response phase but increased, albeit partially, in the revascularization phase (Figures 2D–2F). *Postn* and *Acta2* (αSMA) transcripts strongly correlated in a treatment-independent manner (Figure 2G), corroborating the notion that stromal cells are the key source of POSTN in PNETs. Recombinant POSTN enhanced the proliferation of NIH 3T3 fibroblasts *in vitro* (Figure S2D), suggesting that POSTN may promote stromal cell survival or expansion in an autocrine fashion.

To examine the involvement of POSTN in PNET response to VEGFA inhibition, we crossed *Postn*$^{-/-}$ mice (Malanchi et al., 2011) with RIP1-Tag2 mice. PNETs of *Postn*$^{-/-}$ RIP1-Tag2 mice had a delayed angiogenic switch (Figure S1) and were less vascularized, but they were similar in size compared to PNETs of wild-type (WT) mice (Figures 2H–2K). B20 did not further decrease the relative vascular area, but there was no evidence for rebound angiogenesis at 6 weeks PTI in *Postn*$^{-/-}$ PNETs. Moreover, PNETs of B20-treated *Postn*$^{-/-}$ mice were significantly smaller at 6 weeks PTI than those of IgG-treated *Postn*$^{-/-}$ mice at 4 weeks PTI, suggesting the occurrence of bona fide tumor regressions. Interestingly, *Postn* deficiency suppressed the recovery of αSMA$^+$ stromal cells observed in recalcitrant, B20-treated WT PNETs (Figure 2L). This was accompanied by abated levels of tenascin-C (*Tnc*) and basic fibroblast growth factor (*Fgf2*), which have been previously implicated in PNET angiogenesis (Saupe et al., 2013) and evasion from anti-VEGFA therapy (Casanovas et al., 2005), respectively. Together, these findings indicate that POSTN is required to sustain PNET revascularization and progression during anti-VEGFA therapy.

VEGFA Blockade Augments M2-like PNET-Associated Macrophages in a POSTN-Dependent Manner

Rebounds of proangiogenic myeloid cells may support tumor revascularization during antiangiogenic treatment (Bergers and Hanahan, 2008; De Palma et al., 2017; De Palma and Lewis, 2013; Shojaei and Ferrara, 2008). While F4/80$^+$ macrophage infiltration decreased in WT PNETs during the response phase, it recovered during the revascularization phase, as shown by both immunostaining (Figures 3A and 3B) and qPCR analysis of the macrophage-specific *Emr1* (F4/80) gene (Figure 3C). Intratumoral Ly6C^{high} monocytes and Ly6G$^+$

(4 weeks PTI): n = 11 from 4 mice; anti-VEGFA (4 weeks PTI): n = 35 from 3 mice; anti-VEGFA (6 weeks PTI): n = 25 from 3 mice. Each dot represents one PNET. Statistical analysis by one-way ANOVA with Tukey's multiple comparisons test.

(G) Representative images of CD31 (green) and POSTN (red) immunostaining, and DAPI (blue) nuclear staining, in PNETs of 15- to 17-week-old mice. Scale bar, 100 μm.

(H) Relative POSTN$^+$ area (mean percentage values ± SEM) in 15- to 17-week-old mice. IgG control (4 weeks PTI): n = 18 tumors from 3 mice; anti-VEGFA (4 weeks PTI): n = 37 from 3 mice; anti-VEGFA (6 weeks PTI): n = 34 from 4 mice. Statistical analysis by one-way ANOVA with Tukey's multiple comparisons test.

(I) qPCR analysis of *Postn* in PNETs of 15- to 17-week-old mice. IgG control (4 weeks PTI): n = 18 tumors; anti-VEGFA (4 weeks PTI): n = 22; anti-VEGFA (6 weeks PTI): n = 18. The mean fold change (±SEM) over the reference value (IgG control, set to 1) is shown. *Hprt1* and *B2m* were used as normalizer genes. Data show 2 independent experiments combined; each dot represents one PNET. Statistical analysis by one-way ANOVA with Tukey's multiple comparisons test.

(J) qPCR analysis of *Postn* in PNETs of 12.5- (left) or 13.5-week-old (right) mice. The data were analyzed as in (I). IgG control (1.5 weeks PTI): n = 5 tumors; anti-VEGFA (1.5 weeks PTI): n = 8; IgG control (2.5 weeks PTI): n = 8; anti-VEGFA (2.5 weeks PTI): n = 16. Statistical analysis by Student's two-tailed t test.

See also Figure S1.

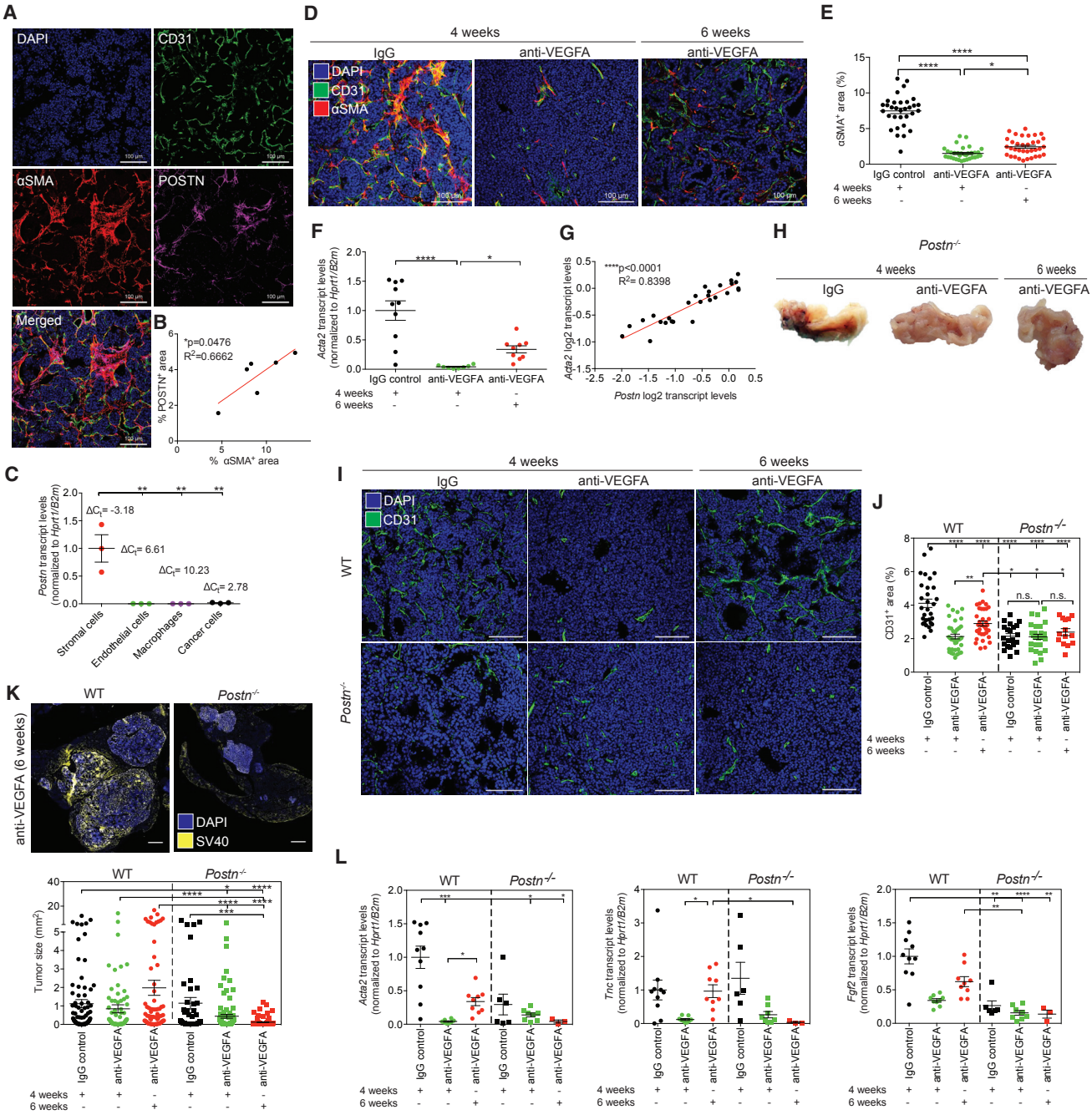

Figure 2. POSTN Is Expressed by Stromal Cells and Sustains PNET Revascularization during VEGFA Blockade

(A) Representative images of CD31 (green), αSMA (red), and POSTN (purple) immunostaining, and DAPI (blue) nuclear staining, in a PNET of a IgG-treated, 15-week-old mouse. Scale bar, 100 μm.

(B) Pearson correlation analysis of POSTN$^+$ and αSMA$^+$ area in PNETs (n = 6) of a 15-week-old IgG-treated mouse.

(C) qPCR-based analysis of *Postn* in cells FACS sorted from PNETs of 15-week-old mice (n = 3). Each dot represents one mouse (several PNETs pooled). The mean fold change (±SEM) over the reference value (stromal cells) is shown. Statistical analysis by one-way ANOVA with Tukey's multiple comparisons test.

(D) Representative images of CD31 (green) and α-SMA (red) immunostaining, and DAPI (blue) nuclear staining, in PNETs of 15- to 17-week-old mice. Scale bar, 100 μm.

(E) Relative αSMA$^+$ area (mean percentage values ± SEM) in PNETs of 15- to 17-week-old mice. IgG control (4 weeks PTI): n = 32 tumors from 5 mice; anti-VEGFA (4 weeks PTI): n = 33 from 3 mice; anti-VEGFA (6 weeks PTI): n = 35 from 4 mice. Statistical analysis by one-way ANOVA with Tukey's multiple comparisons test.

(F) qPCR analysis of *Acta2* (αSMA) in PNETs of 15- to 17-week-old mice. The data were analyzed as in Figure 1I. IgG control (4 weeks PTI): n = 10 tumors; anti-VEGFA (4 weeks PTI): n = 8; anti-VEGFA (6 weeks PTI): n = 9. Statistical analysis by Kruskal-Wallis test with Dunn's multiple comparisons test.

(legend continued on next page)

neutrophils also decreased during the response phase, but they increased only slightly during the revascularization phase (Figure 3D).

Tumor infiltration by CD45$^+$ hematopoietic cells was similar in IgG-treated WT and *Postn*$^{-/-}$ PNETs (Figure 3E). However, the relative proportions of CD11b$^+$ myeloid cells, F4/80$^+$ macrophages, Ly6C^{high} monocytes, and Ly6G$^+$ neutrophils were lower, and those of natural killer (NK) cells and lymphocytes (including CD4$^+$ and CD8$^+$ subsets) higher, in *Postn*$^{-/-}$ compared to WT PNETs, which was indicative of a myeloid-to-lymphoid cell skewing in *Postn*$^{-/-}$ PNETs. Interestingly, B20 decreased the proportions of NK cells in *Postn*$^{-/-}$ PNETs (Figure S3A). Contrary to findings in WT mice, F4/80$^+$ macrophages did not recover in *Postn*$^{-/-}$ PNETs after extended B20 treatment (Figure 3B), a result that may explain the lack of tumor revascularization in *Postn*$^{-/-}$ mice.

Macrophages were present in the exocrine pancreas of both WT and *Postn*$^{-/-}$ RIP1-Tag2 mice (Figure S3B). Also, the relative proportions of CD11b$^+$ myeloid cells, Ly6G$^+$ neutrophils, and Ly6C^{high} monocytes were similar in the peripheral blood of *Postn*$^{-/-}$ and WT mice treated with B20 for 6 weeks (Figure S3C). These data indicate that genetic loss of *Postn* impairs myeloid cell rebounds to B20-treated PNETs without detectably altering myelopoiesis or tissue-resident macrophages.

Consistent with impaired macrophage infiltration in *Postn*$^{-/-}$ PNETs, we observed positive correlations between *Postn* expression and macrophage abundance in WT PNETs by both qPCR and immunostaining (Figures 3F and 3G). Macrophages preferentially localized to POSTN-rich PNET areas (Figure 3H). Also, recombinant POSTN enhanced the migration of immortalized bone marrow macrophages (iBMMs) (Squadrito et al., 2014) in a Transwell assay (Figure S3D). Thus, POSTN may function as a macrophage chemoattractant or survival factor in PNETs.

Tumor macrophages encompass phenotypically defined subsets with nuanced roles in tumor progression; at the extremes of the spectrum are CD11c^{high}MRC1^{low} M1-like macrophages, which have more marked proinflammatory properties, and MRC1^{high}CD11c^{low} M2-like macrophages, which display proangiogenic and protumoral functions (Baer et al., 2016; De Palma and Lewis, 2013). We then analyzed the expression of M1- and M2-associated markers in POSTN-proficient PNETs by flow cytometry, as described previously (Baer et al., 2016). Although B20 did not alter the relative proportion of M1-like macrophages within the parental population, it increased that of M2-like macrophages specifically during the revascularization phase (Figure 3I). Accordingly, qPCR showed enhanced expression of arginase-1 (*Arg1*) and decreased expression of inducible nitric oxide synthetase (*Nos2*) in B20-treated PNETs, suggesting the occurrence of M2-like macrophage skewing during anti-VEGFA therapy (Figure 3J). These results argue that rebound angiogenesis in B20-treated PNETs may be associated with POSTN-dependent, *de novo* recruitment or local expansion of M2-like macrophages.

Pharmacological Elimination of Macrophages through CSF1R Blockade Limits PNET Revascularization during Anti-VEGFA Therapy

To examine the involvement of macrophages in PNET revascularization during VEGFA blockade, we used 2G2, a colony-stimulating factor-1 receptor (CSF1R) mAb that efficiently depletes tumor macrophages in mice (Baer et al., 2016; Ries et al., 2014). Although CSF1R blockade eliminated the majority of tumor macrophages according to both flow cytometry (Figure 4A) and immunostaining (Figures 4B and 4C), it did not extend mouse survival beyond 4 weeks PTI and only moderately reduced the relative CD31$^+$ vascular area in the PNETs (Figures 4B and 4D). As expected, 2G2 abated PNET expression of *Cxcl9* (Figure 3J), a T cell chemokine preferentially produced by macrophages in mouse tumors (Baer et al., 2016).

The combination of 2G2 and B20 prevented M2-like macrophage rebounds after extended antiangiogenic therapy (Figure 4A), decreased *Arg1* expression (Figure 3J), and provided additive antiangiogenic effects compared to B20 monotherapy (Figures 4B and 4D). Importantly, it also abated the incidence of hemorrhagic PNETs (Figure 4E) and impaired tumor growth, as shown by the lack of tumor progression between 4 and 6 weeks PTI (Figure 4F). Of note, macrophage elimination did not alter POSTN expression in WT PNETs (Figures 4G and 4H), arguing that macrophages intervene downstream to stromal cell-derived POSTN in this process. In summary, targeting

(G) Pearson correlation analysis of *Postn* and *Acta2* in PNETs of panel (F).
(H) Representative photos of pancreata of either 15- or 17-week-old *Postn*$^{-/-}$ RIP1-Tag2 mice.
(I) Representative images of CD31 (green) immunostaining and DAPI (blue) nuclear staining in PNETs of 15-17-week-old WT or *Postn*$^{-/-}$ mice. Scale bar, 100 μm.
(J) Relative CD31$^+$ vascular area (mean percentage values ± SEM) in 15- to 17-week-old WT or *Postn*$^{-/-}$ mice. WT mice, IgG control (4 weeks PTI): n = 30 tumors from 4 mice; anti-VEGFA (4 weeks PTI): n = 37 from 4 mice; anti-VEGFA (6 weeks PTI): n = 34 from 4 mice. *Postn*$^{-/-}$ mice, IgG control (4 weeks PTI): n = 21 from 3 mice; anti-VEGFA (4 weeks PTI): n = 27 from 4 mice; anti-VEGFA (6 weeks PTI): n = 14 from 3 mice. Each dot represents one PNET. Statistical analysis by one-way ANOVA using Tukey's multiple comparisons test.
(K) Top: representative images of the SV40 T-Ag (yellow) immunostaining and DAPI (blue) nuclear staining in pancreatic sections of B20-treated, 17-week-old WT or *Postn*$^{-/-}$ mice. Scale bar, 500 μm. Bottom: area of individual T-Ag$^+$ islets/tumors (mean values ± SEM) scored in in the largest pancreatic section of 15- to 17-week-old WT or *Postn*$^{-/-}$ mice. WT mice, IgG control (4 weeks PTI): n = 87 islets/tumors from 4 mice; anti-VEGFA (4 weeks PTI): n = 79 from 2 mice; anti-VEGFA (6 weeks PTI): n = 74 from 3 mice. *Postn*$^{-/-}$ mice, IgG control (4 weeks PTI): n = 42 from 3 mice; anti-VEGFA (4 weeks PTI): n = 97 from 5 mice; anti-VEGFA (6 weeks PTI): n = 82 from 4 mice. Statistical analysis by Kruskal-Wallis test with Dunn's multiple comparisons test.
(L) qPCR analysis of the indicated genes in PNETs of 15- to 17-week-old mice. The data were analyzed as in Figure 1I. IgG control (4 weeks PTI): n = 10 tumors; anti-VEGFA (4 weeks PTI): n = 8; anti-VEGFA (6 weeks PTI): n = 9. *Postn*$^{-/-}$ mice, IgG control (4 weeks PTI): n = 6 tumors; anti-VEGFA (4 weeks PTI): n = 8; anti-VEGFA (6 weeks PTI): n = 3. Note that some of the data (*Acta2*, WT) are also shown in Figure 2F. Statistical analysis by Kruskal-Wallis test with Dunn's multiple comparisons test.
See also Figures S1 and S2.

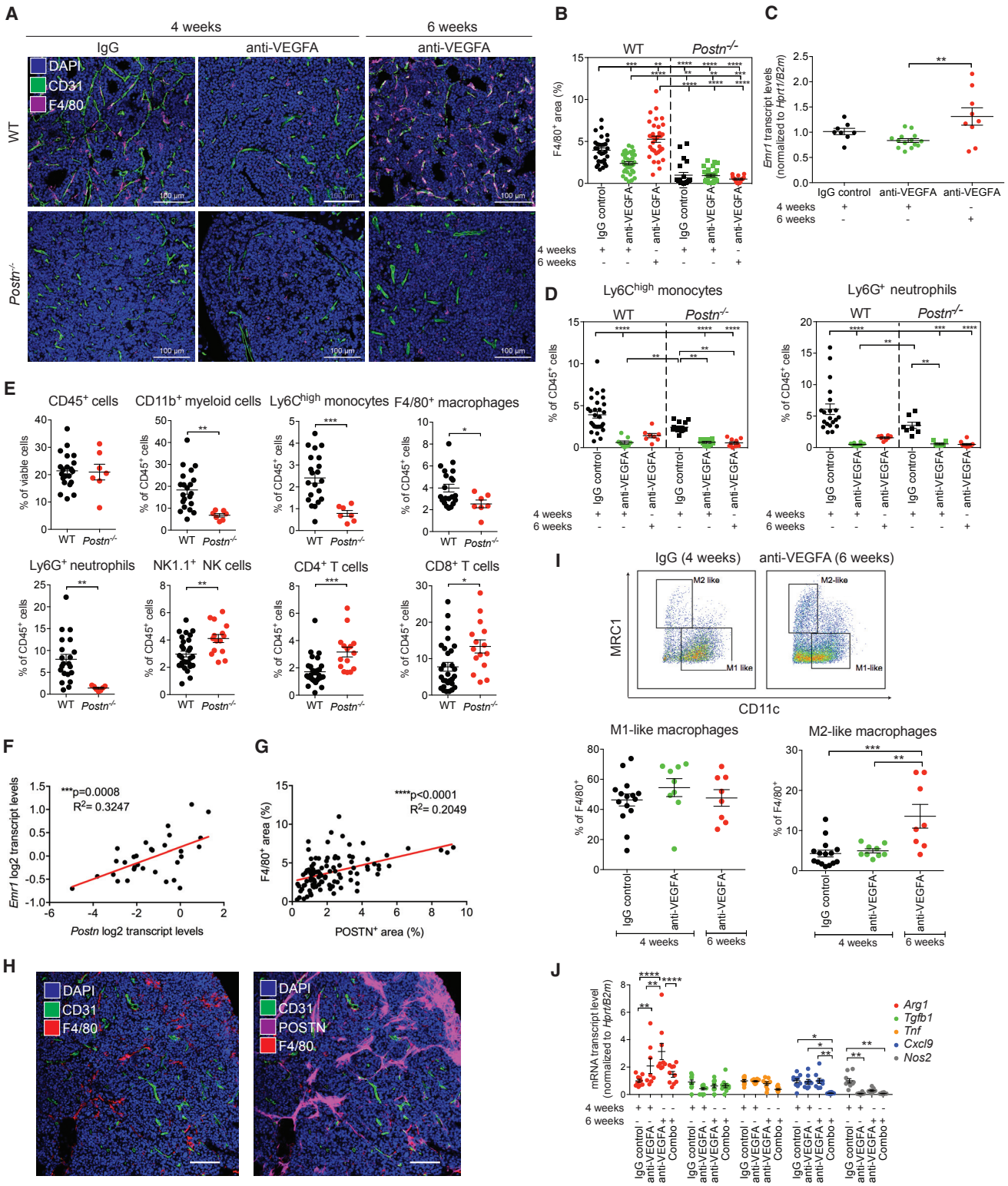

Figure 3. Extended VEGFA Blockade Augments M2-like Tumor Macrophages in a POSTN-Dependent Manner

(A) Representative images of CD31 (green) and F4/80 (purple) immunostaining, and DAPI (blue) nuclear staining, in PNETs of 15- to 17-week-old WT or *Postn*$^{-/-}$ RIP1-Tag2 mice. Scale bar, 100 µm.

(legend continued on next page)

macrophages can extend the therapeutic window of VEGFA blockade in mouse PNETs.

POSTN Correlates with Expression of M2-like Macrophage Genes in Human Pancreatic Endocrine Tumors

We finally examined a cohort of untreated, human primary pancreatic endocrine tumors (Missiaglia et al., 2010; Sadanandam et al., 2015). *POSTN* positively correlated with genes preferentially expressed in M2-like macrophages (*MRC1*, *CD209*, and *CD163*; Figure 4I), but not with genes broadly expressed in macrophages or upregulated in the M1-like subset (*CXCL9*, *CXCL10*, *TNFA*, *IL6*, *IL1B*, and *NOS2*; Figure S4). These data suggest an association between *POSTN* expression and infiltration of M2-like macrophages in human pancreatic endocrine tumors.

DISCUSSION

We report that PNET revascularization and progression under extended VEGFA blockade is associated with enhanced stromal expression of POSTN and recruitment of M2-polarized macrophages in RIP1-Tag2 mice. We observed positive correlations between POSTN and M2-associated macrophage markers, both in mouse and human PNETs, suggesting that POSTN can function as a key macrophage chemoattractant in this tumor type. The genetic deletion of *Postn* blunted macrophage recruitment or survival, impeded rebound angiogenesis, and blocked PNET progression during anti-VEGFA therapy. These findings highlight a mechanism of tumor adaptation to antiangiogenic therapy that is dependent, at least in part, on ECM-regulated macrophages.

Distinct mechanisms of resistance to anti-VEGFA therapy have been described that involve preexisting or induced proangiogenic growth factors (Casanovas et al., 2005; Crawford et al., 2009; Rigamonti et al., 2014; Schmittnaegel et al., 2017). Recent findings also suggest that perturbation of the ECM during VEGFA signaling blockade may curb the efficacy of anticancer treatments. For example, VEGFA inhibition in a mouse model of colorectal liver metastasis enhanced tumor deposition of hyaluronic acid and sulfated glycosaminoglycans, which in turn increased tumor stiffness and limited drug perfusion (Rahbari et al., 2016). Similarly, heightened deposition of fibrillar ECM proteins and elevated expression of lysyl oxydases, which have roles in collagen cross-linking, have been associated with impeded drug permeation and tumor refractoriness to anti-VEGFA therapy (Röhrig et al., 2017).

In our study, VEGFA neutralization reduced the abundance of αSMA$^+$ stromal cells encompassing fibroblasts and pericytes in the PNETs. This agrees with previous work showing that inhibition of VEGFRs disrupts αSMA$^+$ pericytes in PNETs of RIP1-Tag2 mice (Inai et al., 2004). Stromal cell depletion in response to VEGFA signaling inhibition may be secondary to acute vascular pruning, as ECs provide survival cues for pericytes (Franco et al., 2011). Although stromal cell abundance remained low throughout the treatment window, it increased detectably during the revascularization phase. Assuming that VEGFA had been chronically and exhaustively blocked in the PNETs of B20-treated mice, the partial recovery of stromal cells might be explained by VEGFA-independent cues emanating from the revascularizing tumors. These may include FGF2, whose expression was upregulated, in agreement with previous findings (Casanovas et al., 2005). Also, POSTN may promote stromal cell survival and expansion (Xu et al., 2016) in an autocrine fashion

(B) Relative F4/80$^+$ area (mean percentage values ± SEM) in PNETs of 15- to 17-week-old WT or *Postn*$^{-/-}$ mice. WT mice, IgG control (4 weeks PTI): n = 30 tumors from 4 mice; anti-VEGFA (4 weeks PTI): n = 37 from 4 mice; anti-VEGFA (6 weeks PTI): n = 34 from 3 mice. *Postn*$^{-/-}$ mice, IgG control (4 weeks PTI): n = 21 from 3 mice; anti-VEGFA (4 weeks PTI): n = 27 from 4 mice; anti-VEGFA (6 weeks PTI): n = 14 from 3 mice. Statistical analysis by one-way ANOVA with Tukey's multiple comparisons test.

(C) qPCR analysis of *Emr1* in PNETs of 15- to 17-week-old WT mice. The data were analyzed as in Figure 1I. IgG control: n = 8 tumors; anti-VEGFA (4 weeks PTI): n = 14; anti-VEGFA (6 weeks PTI: n = 9. Statistical analysis by one-way ANOVA with Tukey's multiple comparisons test.

(D) Flow cytometry analysis of Ly6C^{high} monocytes (left) and Ly6G$^+$ neutrophils (right) in PNETs of WT or *Postn*$^{-/-}$ mice. Data show the percentage (mean values ± SEM) of the indicated cells among the viable CD45$^+$ cells. Ly6C^{high} monocytes, WT mice: IgG control (4 weeks PTI): n = 29 tumors from 5 mice; anti-VEGFA (4 weeks PTI): n = 9 from 4 mice; anti-VEGFA (6 weeks PTI): n = 8 from 3 mice. Ly6C^{high} monocytes, *Postn*$^{-/-}$ mice: IgG control (4 weeks PTI): n = 15 from 4 mice; anti-VEGFA (4 weeks PTI): n = 12 from 4 mice; anti-VEGFA (6 weeks PTI): n = 10 from 4 mice. Ly6G$^+$ neutrophils, WT mice: IgG control (4 weeks PTI): n = 20 from 5 mice; anti-VEGFA (4 weeks PTI): n = 12 from 3 mice; anti-VEGFA (6 weeks PTI): n = 8 from 2 mice. Ly6G$^+$ neutrophils, *Postn*$^{-/-}$ mice: IgG control (4 weeks PTI): n = 8 from 3 mice; anti-VEGFA (4 weeks PTI): n = 7 from 4 mice; anti-VEGFA (6 weeks PTI): n = 10 from 3 mice. Statistical analysis by Kruskal-Wallis test with Dunn's multiple comparisons test.

(E) Flow cytometry of hematopoietic cells in PNETs of 15-week-old WT (n = 10) or *Postn*$^{-/-}$ (n = 6) mice. Data show the percentage (mean values ± SEM) of the indicated cell types in WT PNETs (n = 21 or 29) or *Postn*$^{-/-}$ PNETs (n = 7 or 15). Data combine two independent experiments. Statistical analysis by Student's t test.

(F and G) Pearson correlation analysis of *Postn* and *Emr1* (F) or POSTN$^+$ and F4/80$^+$ area (G) in PNETs of 15- to 17-week-old WT mice. Data combine PNETs from IgG- and B20-treated mice.

(H) Representative images of CD31 (green), F4/80(red), and POSTN (purple) immunostaining, and DAPI (blue) nuclear staining, in a PNET of a 15-week-old WT mouse. Scale bar, 75 μm.

(I) Top: Flow cytometry analysis of M1-like (CD11c^{high}MRC1^{low}) and M2-like (MRC1^{high}CD11c^{low}) macrophages in PNETs. Bottom panels show the percentage (mean values ± SEM) of F4/80$^+$ TAMs that express an M1-like (left) or M2-like (right) phenotype in PNETs of 15- to 17-week-old WT mice. IgG control (4 weeks PTI): n = 15 tumors from 4 mice; anti-VEGFA (4 weeks PTI): n = 9 from 2 mice; anti-VEGFA (6 weeks PTI): n = 8 from 3 mice. Statistical analysis by one-way ANOVA with Tukey's multiple comparisons test.

(J) qPCR analysis of the indicated genes in PNETs of 15- to 17-week-old WT mice. IgG control: n = 10 tumors; anti-VEGFA (4 weeks PTI): n = 8; anti-VEGFA (6 weeks PTI): n = 9; anti-VEGFA plus anti-CSF1R (Combo; 6 weeks PTI): n = 10. The data were analyzed as in Figure 1I. Statistical analysis by two-way ANOVA with Tukey's multiple comparisons test.

See also Figure S3.

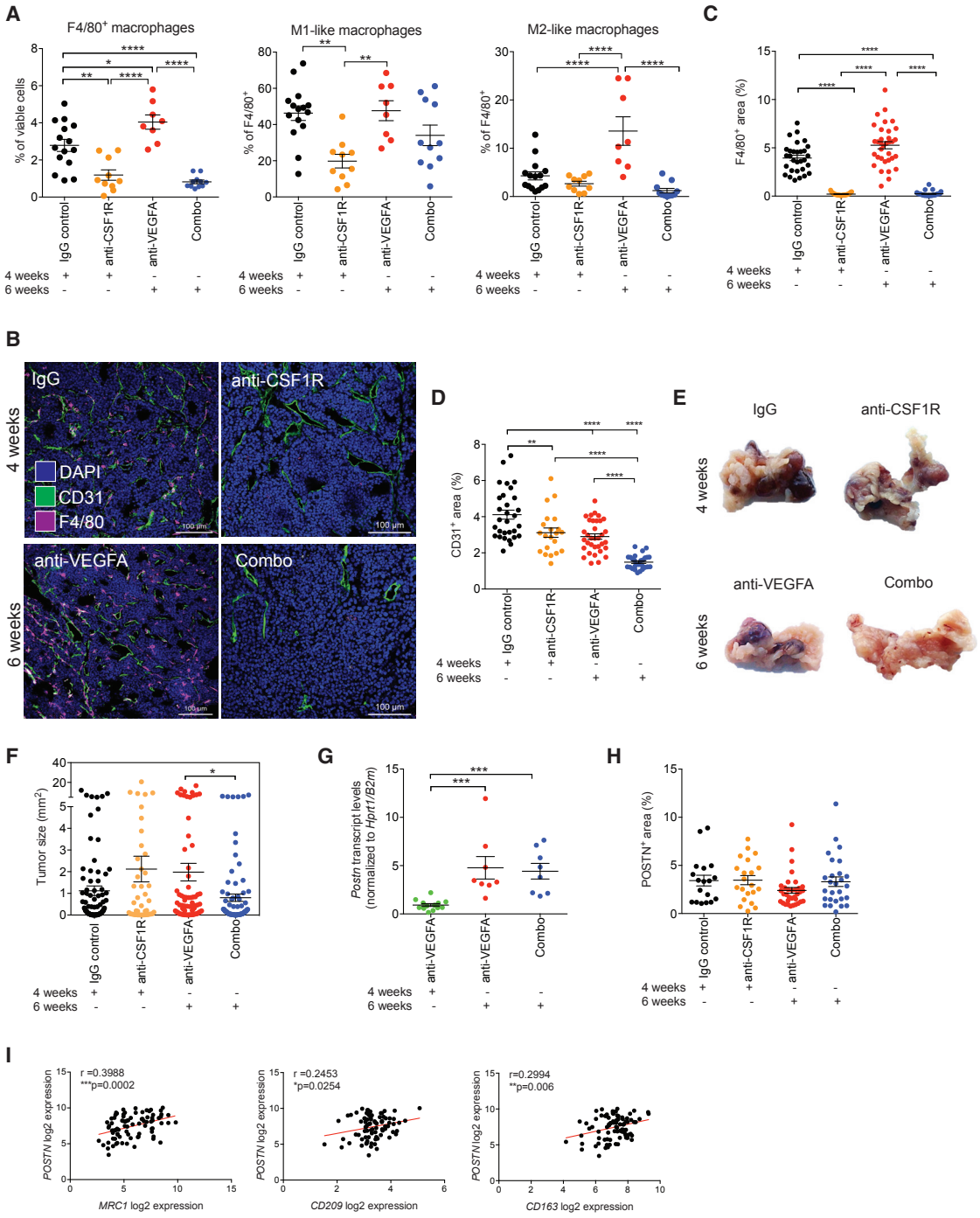

Figure 4. Macrophages Limit PNET Response to VEGFA Blockade

(A) Percentage (mean values ± SEM) of total (F4/80$^+$), M1-like, and M2-like macrophages in PNETs of 15- to 17-week-old WT mice. IgG control (4 weeks PTI): n = 15 tumors from 4 mice; anti-CSF1R (4 weeks PTI): n = 10 from 4 mice; anti-VEGFA (6 weeks PTI): n = 8 from 3 mice; anti-VEGFA plus anti-CSF1R (Combo; 6 weeks PTI): n = 11 from 3 mice. Statistical analysis by one-way ANOVA with Tukey's multiple comparisons test. Some of data are also shown in Figure 3I.

(B) Representative images of CD31 (green) and F4/80 (purple) immunostaining, and DAPI (blue) nuclear staining, in PNETs of 15- to 17-week-old WT mice. Scale bar, 100 µm.

(C and D) Relative F4/80$^+$ (C) or CD31$^+$ (D) area (mean percentage values ± SEM) in PNETs of 15- to 17-week-old WT mice. IgG control (4 weeks PTI): n = 30 tumors from 4 mice; anti-CSF1R (4 weeks PTI) n = 21 from 4 mice; anti-VEGFA (6 weeks PTI): n = 34 from 4 mice; anti-VEGFA plus anti-CSF1R (Combo; 6 weeks PTI): n = 27 from 4 mice. Note that some of the data in (C) (WT mice: IgG control and anti-VEGFA at 6 weeks) are also shown in Figure 3B; some of the data in

(legend continued on next page)

in VEGFA-depleted microenvironments. Our results indicate that αSMA$^+$ stromal cells are the main source of POSTN in the PNETs, as shown previously in other tumor types (Kikuchi et al., 2014; Underwood et al., 2015). Although the mechanism(s) regulating POSTN production by tumor-associated stromal cells in the context of VEGFA blockade remain unclear, our data support a model whereby lingering stromal cells sustain POSTN deposition in revascularizing PNETs.

POSTN expression correlated with, and its genetic deletion abated, macrophage abundance in both untreated and anti-VEGFA treated PNETs. These findings suggest that POSTN may function as a macrophage chemoattractant in PNETs. Accordingly, glioblastoma-associated POSTN recruits and polarizes macrophages to an M2-like phenotype through $\alpha_v\beta_3$ integrin (Zhou et al., 2015). Our analysis of human PNET datasets indicates that *POSTN* gene expression correlates with M2-macrophage markers. These results support the notions that POSTN promotes M2-like macrophage recruitment and polarization in human PNETs, and that this phenomenon may contribute, at least partly, to human PNET refractoriness or adaptive resistance to VEGFA signaling inhibitors. These findings encourage the clinical testing of combined CSF1R and VEGFA blockade in patients with cancer (https://www.clinicaltrials.gov identifier NCT02923739).

Remarkably, VEGFA inhibition blocked PNET progression in *Postn*-deficient mice. Further to blunting macrophage rebounds in B20-treated PNETs, POSTN deficiency attenuated basal and therapy-induced tumor infiltration by neutrophils and monocytes, which have proangiogenic and immunosuppressive functions in the context of antiangiogenic therapy (Rivera and Bergers, 2015; Rivera et al., 2015; Shojaei and Ferrara, 2008). Moreover, it impeded the surge, induced by VEGFA blockade, of FGF2, which was previously implicated in PNET evasion from VEGFA signaling inhibition (Casanovas et al., 2005). Owing to these effects on multiple cellular targets, the outcome of *Postn* inactivation on PNET revascularization and progression during extended VEGFA therapy was more robust than that of selective macrophage elimination in *Postn*-proficient PNETs. These findings and considerations suggest broad roles for POSTN in orchestrating multifaceted mechanisms of tumor adaptation to anti-VEGFA therapy.

EXPERIMENTAL PROCEDURES

Detailed experimental procedures are presented in Supplemental Experimental Procedures.

Study Design

This study was designed to investigate the role of POSTN in PNET response to VEGFA blockade. To this aim, we used the genetically engineered mouse model of PNET, RIP1-Tag2. All procedures were performed according to protocols approved by the Veterinary Authorities of the Canton Vaud according to Swiss law (protocols 2574 and 2574.1) or by the ethical committee of Alsace, France (CREMEAS; protocols 04077.02 and E67-482-21).

The generation of transgenic mice and design of treatment trials are presented in Supplemental Experimental Procedures. Briefly, treatment trials were performed by pre-planned enrollment of transgenic mice when they reached a defined age (10.5–11.5 weeks); hence, the mice were often treated independently, and no synchronized experimental cohorts were established. The mice were treated with mAbs for up to 6 weeks, depending on the experimental treatment. Most RIP1-Tag2 mice reach the termination criteria between 15 and 16 weeks of age, with demising health conditions owing to compromised endocrine pancreas function. WT and *Postn*$^{-/-}$ RIP1-Tag2 mice receiving B20 alone or with 2G2 typically gain extended survival, but health conditions eventually deteriorate between 17 and 19 weeks of age, regardless of tumor burden. Thus, we implemented fixed time points of termination at 4 and 6 weeks PTI, depending on the treatment and genetic background. Detailed information on the sample size and statistical methods is presented in the figures and associated legends.

Analytical studies (e.g., quantification of immune cells and vascular parameters, gene expression) were typically performed several times in independent experiments, implementing fixed time points of analysis for all experimental groups, while individual PNETs were analyzed from typically 2–5 mice per group (each pancreas develops multiple tumors; note that *Postn*$^{-/-}$ mice present with few PNETs after VEGFA blockade). Because PNETs develop from normal islets of Langerhans, tumor area data (Figures 2K and 4F) were obtained by analyzing all islets, independent of malignant status, at each fixed time point. Other parameters (e.g., vascularization, expression of cell-associated markers) were analyzed in overt tumors. Fixed time points are shown in the figures and indicate the time elapsed from the treatment start ("PTI").

The investigators were not blinded when assessing the results or analyzing data. On rare occasions, outliers at the end-point were excluded by using the ROUT method (provided in GraphPad Prism) to identify outliers. In some cases, selected samples were excluded from specific analyses because of technical flaws during sample processing or data acquisition.

Statistical Analysis

Error bars indicate SEM. The number of biological (nontechnical) replicates in each experiment is indicated in the figure legends. Individual PNETs were

(D) (WT mice: IgG control and anti-VEGFA at 6 weeks) are also shown in Figure 2J. Statistical analysis by Kruskal-Wallis test with Dunn's multiple comparisons test (C), or one-way ANOVA with Tukey's multiple comparisons test (D).
(E) Representative photos of pancreata of either 15- or 17-week-old WT mice.
(F) Area of individual T-Ag$^+$ islets/tumors (mean values ± SEM) scored in the largest pancreatic section of 15- to 17-week-old WT mice. IgG control (4 weeks PTI): n = 87 islet/tumors from 4 mice; anti-CSF1R (4 weeks PTI) n = 44 from 4 mice; anti-VEGFA (6 weeks PTI): n = 74 from 3 mice; anti-VEGFA plus anti-CSF1R (Combo; 6 weeks PTI): n = 87 from 4 mice. Note that some of the data (WT mice: IgG control and anti-VEGFA at 6 weeks) are also shown in Figure 2K. Statistical analysis by Kruskal-Wallis test with Dunn's multiple comparisons test.
(G) qPCR analysis of *Postn* in PNETs of 15- to 17-week-old mice. The data were analyzed as in Figure 1I. Anti-VEGFA (4 weeks PTI): n = 13 tumors; anti-VEGFA (6 weeks PTI): n = 8; anti-VEGFA plus anti-CSF1R (Combo; 6 weeks PTI): n = 8. Statistical analysis was performed using Kruskal-Wallis test with Dunn's multiple comparisons test.
(H) Relative POSTN$^+$ area (mean percentage values ± SEM) in PNETs of 15- to 17-week-old mice. IgG control (4 weeks PTI): n = 18 tumors from 3 mice; anti-CSF1R (4 weeks PTI) n = 21 from 4 mice; anti-VEGFA (6 weeks PTI): n = 34 from 4 mice; anti-VEGFA plus anti-CSF1R (Combo; 6 weeks PTI): n = 27 from 4 mice. Note that some of the data in (H)(WT mice: IgG control and anti-VEGFA at 6 weeks) are also shown in Figure 1H. Statistical analysis was performed using Kruskal-Wallis test with Dunn's multiple comparisons test.
(I) Pearson correlation analysis of *POSTN* and M2-associated genes in human pancreatic endocrine tumors. Data were extracted from published microarray data (GSE73338). Each point represents one tumor.
See also Figure S4.

considered as independent samples, as they develop independently (and respond variably to therapy) in the pancreas of each mouse. Statistical analysis of experiments with more than 2 groups used one-way ANOVA with Tukey's correction for multiple comparisons when the data were normally distributed according to D'Agostino-Pearson omnibus test, as implemented in the Prism statistical software, or the Kruskal-Wallis test with Dunn's multiple comparisons test when the data were not normally distributed. For experiments with 2 groups, statistical analysis used Student's t test with a 95% confidence interval. Correlation analyses were performed using Pearson's correlation.

Statistical differences are indicated as follows: *, $0.01 \leq p < 0.05$; **, $0.001 \leq p < 0.01$; ***, $0.0001 \leq p < 0.001$; ****, $p < 0.0001$.

SUPPLEMENTAL INFORMATION

Supplemental Information includes Supplemental Experimental Procedures and four figures and can be found with this article online at https://doi.org/10.1016/j.celrep.2018.02.035.

ACKNOWLEDGMENTS

We thank C. Wyser-Rmili for maintaining mouse colonies, S. Nassiri for advice on statistics, and M.L. Squadrito for help with artwork. This work was supported by the Swiss Cancer League (grants KFS-3007-08-2012 and KFS-3759-08-2015), the Swiss Bridge (to M.D.P.), and the Agence National pour la Recherche (ANR-AngioMatrix) (to G.O.).

AUTHOR CONTRIBUTIONS

I.K. designed research, performed experiments, collected and analyzed data, interpreted results, and wrote the paper. E.K. performed experiments, analyzed data, and interpreted results. A.B. performed experiments. S.B. and C.H.R. advised on experimental design, provided mAbs, and interpreted results. B.L. and G.O. provided *Postn*$^{-/-}$ mice, analyzed angiogenic islets, and interpreted results. M.D.P. designed and supervised research, interpreted results, and wrote the paper.

DECLARATION OF INTERESTS

S.B. and C.H.R. are Roche employees. C.H.R. filed patent applications on CSF1R blockade for targeting macrophages (WO2011107553A1 and WO2013132044A1). The remaining authors declare no competing interests.

Received: April 15, 2017
Revised: December 23, 2017
Accepted: February 8, 2018
Published: March 6, 2018

REFERENCES

Allen, E., Miéville, P., Warren, C.M., Saghafinia, S., Li, L., Peng, M.-W., and Hanahan, D. (2016). Metabolic symbiosis enables adaptive resistance to anti-angiogenic therapy that is dependent on mTOR signaling. Cell Rep. *15*, 1144–1160.

Baer, C., Squadrito, M.L., Laoui, D., Thompson, D., Hansen, S.K., Kiialainen, A., Hoves, S., Ries, C.H., Ooi, C.-H., and De Palma, M. (2016). Suppression of microRNA activity amplifies IFN-γ-induced macrophage activation and promotes anti-tumour immunity. Nat. Cell Biol. *18*, 790–802.

Bao, S., Ouyang, G., Bai, X., Huang, Z., Ma, C., Liu, M., Shao, R., Anderson, R.M., Rich, J.N., and Wang, X.-F. (2004). Periostin potently promotes metastatic growth of colon cancer by augmenting cell survival via the Akt/PKB pathway. Cancer Cell *5*, 329–339.

Bergers, G., and Hanahan, D. (2008). Modes of resistance to anti-angiogenic therapy. Nat. Rev. Cancer *8*, 592–603.

Bergers, G., Brekken, R., McMahon, G., Vu, T.H., Itoh, T., Tamaki, K., Tanzawa, K., Thorpe, P., Itohara, S., Werb, Z., and Hanahan, D. (2000). Matrix metalloproteinase-9 triggers the angiogenic switch during carcinogenesis. Nat. Cell Biol. *2*, 737–744.

Casanovas, O., Hicklin, D.J., Bergers, G., and Hanahan, D. (2005). Drug resistance by evasion of antiangiogenic targeting of VEGF signaling in late-stage pancreatic islet tumors. Cancer Cell *8*, 299–309.

Chen, G., Nakamura, I., Dhanasekaran, R., Iguchi, E., Tolosa, E.J., Romecin, P.A., Vera, R.E., Almada, L.L., Miamen, A.G., Chaiteerakij, R., et al. (2017). Transcriptional induction of periostin by a sulfatase 2-TGFβ1-SMAD signaling Axis mediates tumor angiogenesis in hepatocellular carcinoma. Cancer Res. *77*, 632–645.

Crawford, Y., Kasman, I., Yu, L., Zhong, C., Wu, X., Modrusan, Z., Kaminker, J., and Ferrara, N. (2009). PDGF-C mediates the angiogenic and tumorigenic properties of fibroblasts associated with tumors refractory to anti-VEGF treatment. Cancer Cell *15*, 21–34.

De Palma, M., and Lewis, C.E. (2013). Macrophage regulation of tumor responses to anticancer therapies. Cancer Cell *23*, 277–286.

De Palma, M., Biziato, D., and Petrova, T.V. (2017). Microenvironmental regulation of tumour angiogenesis. Nat. Rev. Cancer *17*, 457–474.

Egeblad, M., Rasch, M.G., and Weaver, V.M. (2010). Dynamic interplay between the collagen scaffold and tumor evolution. Curr. Opin. Cell Biol. *22*, 697–706.

Ferrara, N., and Adamis, A.P. (2016). Ten years of anti-vascular endothelial growth factor therapy. Nat. Rev. Drug Discov. *15*, 385–403.

Franco, M., Roswall, P., Cortez, E., Hanahan, D., and Pietras, K. (2011). Pericytes promote endothelial cell survival through induction of autocrine VEGF-A signaling and Bcl-w expression. Blood *118*, 2906–2917.

Frentzas, S., Simoneau, E., Bridgeman, V.L., Vermeulen, P.B., Foo, S., Kostaras, E., Nathan, M., Wotherspoon, A., Gao, Z.H., Shi, Y., et al. (2016). Vessel co-option mediates resistance to anti-angiogenic therapy in liver metastases. Nat. Med. *22*, 1294–1302.

Hu, F., Shang, X.-F., Wang, W., Jiang, W., Fang, C., Tan, D., and Zhou, H.-C. (2016). High-level expression of periostin is significantly correlated with tumour angiogenesis and poor prognosis in osteosarcoma. Int. J. Exp. Pathol. *97*, 86–92.

Inai, T., Mancuso, M., Hashizume, H., Baffert, F., Haskell, A., Baluk, P., Hu-Lowe, D.D., Shalinsky, D.R., Thurston, G., Yancopoulos, G.D., and McDonald, D.M. (2004). Inhibition of vascular endothelial growth factor (VEGF) signaling in cancer causes loss of endothelial fenestrations, regression of tumor vessels, and appearance of basement membrane ghosts. Am. J. Pathol. *165*, 35–52.

Kikuchi, Y., Kunita, A., Iwata, C., Komura, D., Nishiyama, T., Shimazu, K., Takeshita, K., Shibahara, J., Kii, I., Morishita, Y., et al. (2014). The niche component periostin is produced by cancer-associated fibroblasts, supporting growth of gastric cancer through ERK activation. Am. J. Pathol. *184*, 859–870.

Langlois, B., Saupe, F., Rupp, T., Arnold, C., van der Heyden, M., Orend, G., and Hussenet, T. (2014). AngioMatrix, a signature of the tumor angiogenic switch-specific matrisome, correlates with poor prognosis for glioma and colorectal cancer patients. Oncotarget *5*, 10529–10545.

Liang, W.-C., Wu, X., Peale, F.V., Lee, C.V., Meng, Y.G., Gutierrez, J., Fu, L., Malik, A.K., Gerber, H.-P., Ferrara, N., and Fuh, G. (2006). Cross-species vascular endothelial growth factor (VEGF)-blocking antibodies completely inhibit the growth of human tumor xenografts and measure the contribution of stromal VEGF. J. Biol. Chem. *281*, 951–961.

Liu, A.Y., Zheng, H., and Ouyang, G. (2014). Periostin, a multifunctional matricellular protein in inflammatory and tumor microenvironments. Matrix Biol. *37*, 150–156.

Malanchi, I., Santamaria-Martínez, A., Susanto, E., Peng, H., Lehr, H.-A., Delaloye, J.-F., and Huelsken, J. (2011). Interactions between cancer stem cells and their niche govern metastatic colonization. Nature *481*, 85–89.

Missiaglia, E., Dalai, I., Barbi, S., Beghelli, S., Falconi, M., della Peruta, M., Piemonti, L., Capurso, G., Di Florio, A., delle Fave, G., et al. (2010). Pancreatic endocrine tumors: expression profiling evidences a role for AKT-mTOR pathway. J. Clin. Oncol. *28*, 245–255.

Naba, A., Clauser, K.R., Mani, D.R., Carr, S.A., and Hynes, R.O. (2017). Quantitative proteomic profiling of the extracellular matrix of pancreatic islets during the angiogenic switch and insulinoma progression. Sci. Rep. *7*, 40495.

Park, S.Y., Piao, Y., Jeong, K.J., Dong, J., and de Groot, J.F. (2016). Periostin (POSTN) regulates tumor resistance to antiangiogenic therapy in glioma models. Mol. Cancer Ther. *15*, 2187–2197.

Rahbari, N.N., Kedrin, D., Incio, J., Liu, H., Ho, W.W., Nia, H.T., Edrich, C.M., Jung, K., Daubriac, J., Chen, I., et al. (2016). Anti-VEGF therapy induces ECM remodeling and mechanical barriers to therapy in colorectal cancer liver metastases. Sci. Transl. Med. *8*, 360ra135.

Ries, C.H., Cannarile, M.A., Hoves, S., Benz, J., Wartha, K., Runza, V., Rey-Giraud, F., Pradel, L.P., Feuerhake, F., Klaman, I., et al. (2014). Targeting tumor-associated macrophages with anti-CSF-1R antibody reveals a strategy for cancer therapy. Cancer Cell *25*, 846–859.

Rigamonti, N., Kadioglu, E., Keklikoglou, I., Wyser Rmili, C., Leow, C.C., and De Palma, M. (2014). Role of angiopoietin-2 in adaptive tumor resistance to VEGF signaling blockade. Cell Rep. *8*, 696–706.

Rivera, L.B., and Bergers, G. (2015). Intertwined regulation of angiogenesis and immunity by myeloid cells. Trends Immunol. *36*, 240–249.

Rivera, L.B., Meyronet, D., Hervieu, V., Frederick, M.J., Bergsland, E., and Bergers, G. (2015). Intratumoral myeloid cells regulate responsiveness and resistance to antiangiogenic therapy. Cell Rep. *11*, 577–591.

Röhrig, F., Vorlová, S., Hoffmann, H., Wartenberg, M., Escorcia, F.E., Keller, S., Tenspolde, M., Weigand, I., Gätzner, S., Manova, K., et al. (2017). VEGF-ablation therapy reduces drug delivery and therapeutic response in ECM-dense tumors. Oncogene *36*, 1–12.

Sadanandam, A., Wullschleger, S., Lyssiotis, C.A., Grötzinger, C., Barbi, S., Bersani, S., Körner, J., Wafy, I., Mafficini, A., Lawlor, R.T., et al. (2015). A cross-species analysis in pancreatic neuroendocrine tumors reveals molecular subtypes with distinctive clinical, metastatic, developmental, and metabolic characteristics. Cancer Discov. *5*, 1296–1313.

Saupe, F., Schwenzer, A., Jia, Y., Gasser, I., Spenlé, C., Langlois, B., Kammerer, M., Lefebvre, O., Hlushchuk, R., Rupp, T., et al. (2013). Tenascin-C downregulates wnt inhibitor dickkopf-1, promoting tumorigenesis in a neuroendocrine tumor model. Cell Rep. *5*, 482–492.

Schmittnaegel, M., Rigamonti, N., Kadioglu, E., Cassará, A., Wyser Rmili, C., Kiialainen, A., Kienast, Y., Mueller, H.-J., Ooi, C.-H., Laoui, D., et al. (2017). Dual angiopoietin-2 and VEGFA inhibition elicits antitumor immunity that is enhanced by PD-1 checkpoint blockade. Sci. Transl. Med. *9*, eaak9670.

Shao, R., Bao, S., Bai, X., Blanchette, C., Anderson, R.M., Dang, T., Gishizky, M.L., Marks, J.R., and Wang, X.-F. (2004). Acquired expression of periostin by human breast cancers promotes tumor angiogenesis through up-regulation of vascular endothelial growth factor receptor 2 expression. Mol. Cell. Biol. *24*, 3992–4003.

Shojaei, F., and Ferrara, N. (2008). Refractoriness to antivascular endothelial growth factor treatment: role of myeloid cells. Cancer Res. *68*, 5501–5504.

Squadrito, M.L., Baer, C., Burdet, F., Maderna, C., Gilfillan, G.D., Lyle, R., Ibberson, M., and De Palma, M. (2014). Endogenous RNAs modulate microRNA sorting to exosomes and transfer to acceptor cells. Cell Rep. *8*, 1432–1446.

Stylianopoulos, T., Martin, J.D., Chauhan, V.P., Jain, S.R., Diop-Frimpong, B., Bardeesy, N., Smith, B.L., Ferrone, C.R., Hornicek, F.J., Boucher, Y., et al. (2012). Causes, consequences, and remedies for growth-induced solid stress in murine and human tumors. Proc. Natl. Acad. Sci. USA *109*, 15101–15108.

Sugimoto, H., Mundel, T.M., Kieran, M.W., and Kalluri, R. (2006). Identification of fibroblast heterogeneity in the tumor microenvironment. Cancer Biol. Ther. *5*, 1640–1646.

Takanami, I., Abiko, T., and Koizumi, S. (2008). Expression of periostin in patients with non-small cell lung cancer: correlation with angiogenesis and lymphangiogenesis. Int. J. Biol. Markers *23*, 182–186.

Underwood, T.J., Hayden, A.L., Derouet, M., Garcia, E., Noble, F., White, M.J., Thirdborough, S., Mead, A., Clemons, N., Mellone, M., et al. (2015). Cancer-associated fibroblasts predict poor outcome and promote periostin-dependent invasion in oesophageal adenocarcinoma. J. Pathol. *235*, 466–477.

Van Obberghen-Schilling, E., Tucker, R.P., Saupe, F., Gasser, I., Cseh, B., and Orend, G. (2011). Fibronectin and tenascin-C: accomplices in vascular morphogenesis during development and tumor growth. Int. J. Dev. Biol. *55*, 511–525.

Xu, X., Chang, W., Yuan, J., Han, X., Tan, X., Ding, Y., Luo, Y., Cai, H., Liu, Y., Gao, X., et al. (2016). Periostin expression in intra-tumoral stromal cells is prognostic and predictive for colorectal carcinoma *via* creating a cancer-supportive niche. Oncotarget *7*, 798–813.

Zhou, W., Ke, S.Q., Huang, Z., Flavahan, W., Fang, X., Paul, J., Wu, L., Sloan, A.E., McLendon, R.E., Li, X., et al. (2015). Periostin secreted by glioblastoma stem cells recruits M2 tumour-associated macrophages and promotes malignant growth. Nat. Cell Biol. *17*, 170–182.

Zhu, M., Fejzo, M.S., Anderson, L., Dering, J., Ginther, C., Ramos, L., Gasson, J.C., Karlan, B.Y., and Slamon, D.J. (2010). Periostin promotes ovarian cancer angiogenesis and metastasis. Gynecol. Oncol. *119*, 337–344.